Electronic Supplementary Material (ESI) for Physical Chemistry Chemical Physics.

Supporting information

Concentration dependence of the up- and down-conversion emission colour of Er^{3+}-doped Y_2O_3; a time-resolved spectroscopy analysis

Haizhou Lu[a], William P. Gillin[a,b]* and Ignacio Hernández[c]*

[a] School of Physics and Astronomy, Queen Mary University of London, Mile End Road, London, E1 4NS, UK

[b] College of Physical Science and Technology, Sichuan University, Chengdu, 610064, People's Republic of China

[c] Dpto. CITIMAC, Universidad de Cantabria, Facultad de Ciencias, Avda. Los Castros, s/n 39005, Santander, Spain

*w.gillin@qmul.ac.uk

*ignacio.hernandez@unican.es

Table of contents:

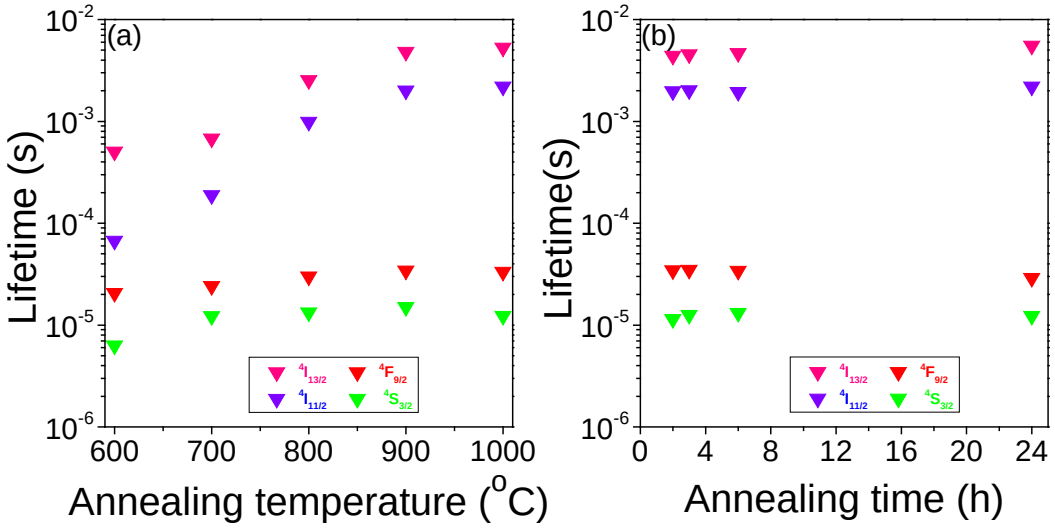

Fig. S1 (a): measured lifetimes of $^4I_{13/2}$, $^4I_{11/2}$, $^4F_{9/2}$ and $^4S_{3/2}$ states of 5% Er^{3+}-doped Y_2O_3 annealed for 24 hours at different temperature with 488 nm OPO laser; (b): measured lifetimes of $^4I_{13/2}$, $^4I_{11/2}$, $^4F_{9/2}$ and $^4S_{3/2}$ states of 5% Er^{3+}-doped Y_2O_3 annealed at 1000 °C for different hours with 488 nm OPO laser (power density is $3\times10^6 W/cm^2$).

(a)

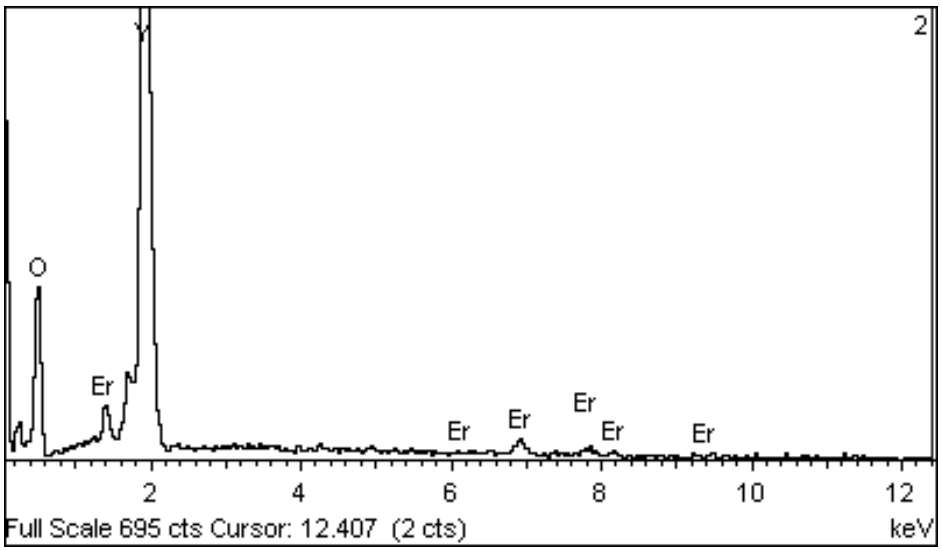

(b)

	0.2% Er^{3+}:Y_2O_3	5% Er^{3+}:Y_2O_3	10% Er^{3+}:Y_2O_3
Er/Y	0.243%	5.97%	9.94%

Fig. S2. (a) Energy disperse X-ray spectroscopy of the 5% Er^{3+}-doped Y_2O_3; (b) the measured elemental ratio of Er/Y of the 0.2%, 5% and 10% Er^{3+}-doped Y_2O_3 samples.

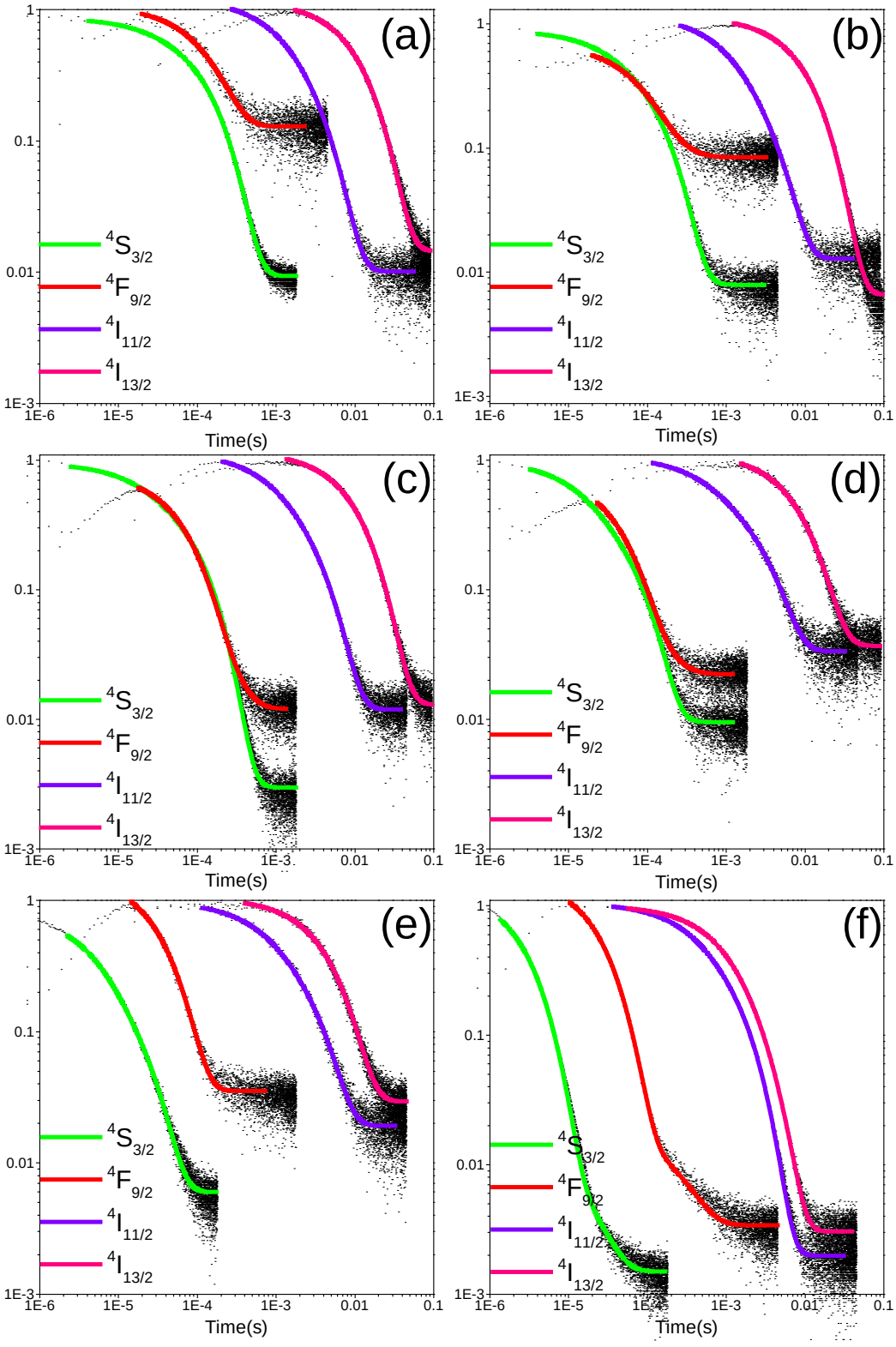

Fig. S3: Intensity decay curves of all emitting states of different concentration doped Er^{3+}-doped Y_2O_3 under 488 nm OPO laser: (a) 0.2%, (b) 0.5%, (c) 1%, (d) 2%, (e) 5%, (f) 10% (power density is 3×10^6 W/cm^2).

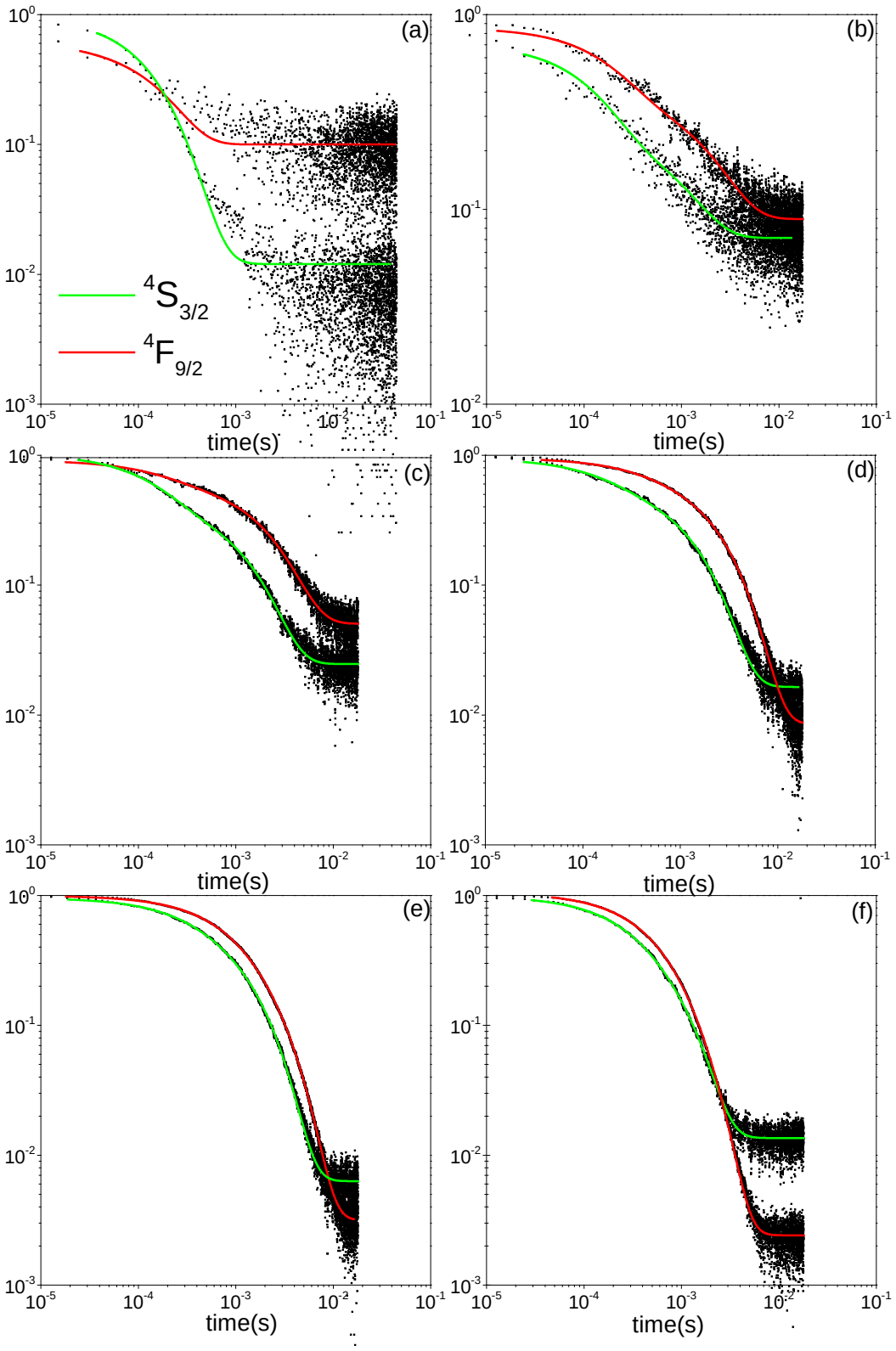

Fig. S4: Intensity decay curves of all emitting states of different concentration doped Er^{3+}-doped Y_2O_3 under 980 nm CW laser: (a) 0.2%, (b) 0.5%, (c) 1%, (d) 2%, (e) 5%, (f) 10% (power density is 50 W/cm^2).

Emission Wavelength (nm)	0.2% Er^{3+}-doping		0.5% Er^{3+}-doping		1% Er^{3+}-doping	
	488 nm OPO	980 nm UC	488 nm OPO	980 nm UC	488 nm OPO	980 nm UC
1535	0.0101		0.00932		0.00952	
980	0.00209		0.00195		0.00212	
660	1.18×10^{-4}	1.48×10^{-4}	1.03×10^{-4}	0.00159	7.94×10^{-5}	0.00191
560	1.18×10^{-4}	1.40×10^{-4}	9.84×10^{-5}	7.45×10^{-4}	7.90×10^{-5}	0.00101

Emission Wavelength (nm)	2% Er^{3+}-doping		5% Er^{3+}-doping		10% Er^{3+}-doping	
	488 nm OPO	980 nm UC	488 nm OPO	980 nm UC	488 nm OPO	980 nm UC
1535	0.00742		0.0044		0.00142	
980	0.00201		0.0019		9.79×10^{-4}	
660	5.16×10^{-5}	0.00212	3.45×10^{-5}	0.00152	6.51×10^{-5}	6.92×10^{-4}
560	4.46×10^{-5}	0.00117	1.14×10^{-5}	0.0011	3.07×10^{-6}	6.02×10^{-4}

Table S1. Average decay times of the emitting states of the studied Er^{3+}-doped Y_2O_3 samples under 488 nm OPO (power density is 3×10^6 W/cm^2) and 980 nm (power density is 50W/cm^2) UC excitation conditions. Numbers (in seconds) correspond to solid symbols in figure 3.

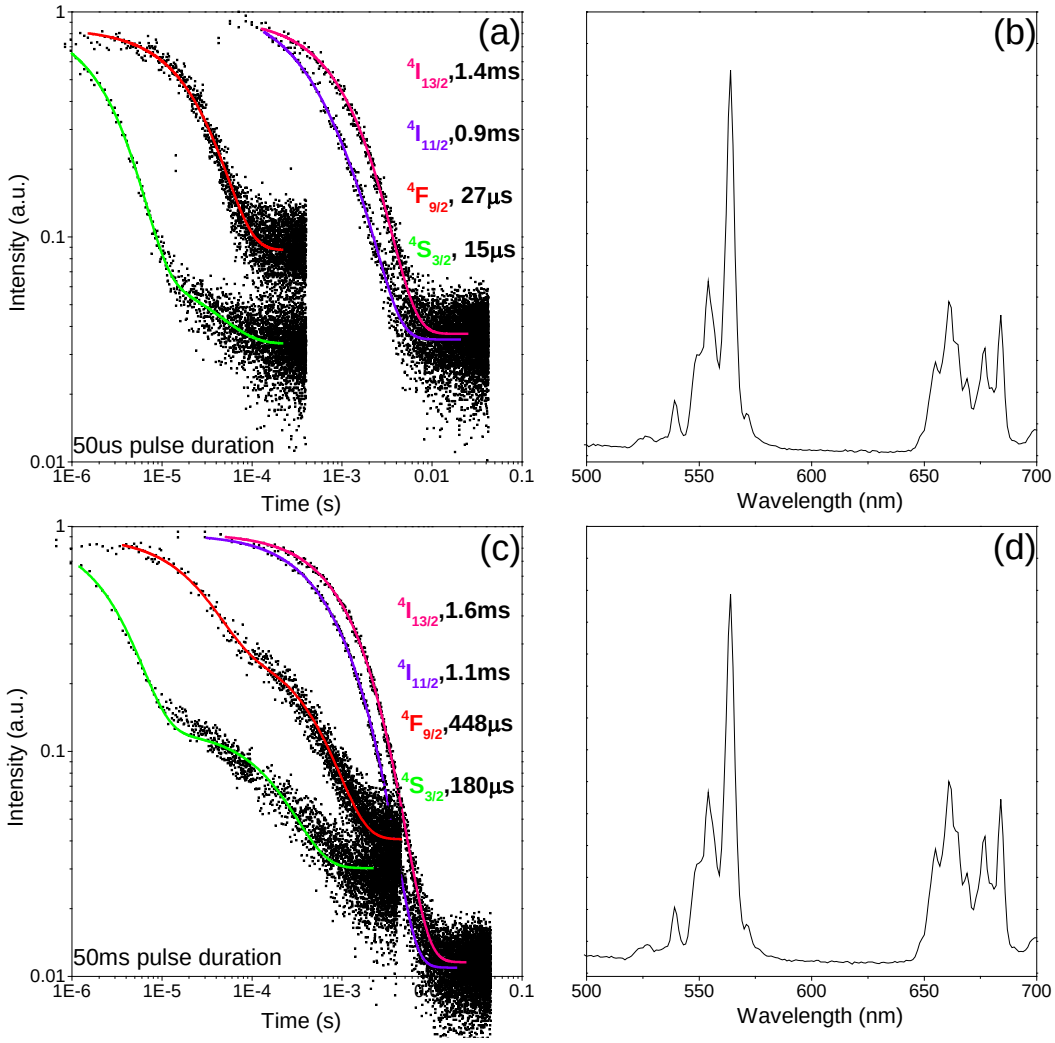

Fig. S5. (a) Intensity decay curves of $^4I_{13/2}$, $^4I_{11/2}$, $^4F_{9/2}$ and $^4S_{3/2}$ states of 10% Er^{3+}-doped Y_2O_3 with 405 CW laser modulated at 50us pulse length; (b) emission spectrum of 10% Er^{3+}-doped Y_2O_3 with 405 CW laser modulated at 50us pulse length; (c) intensity decay curves of $^4I_{13/2}$, $^4I_{11/2}$, $^4F_{9/2}$ and $^4S_{3/2}$ states of 10% Er^{3+}-doped Y_2O_3 with 405 CW laser modulated at 50 ms pulse length; (d) emission spectrum of 10% Er^{3+}-doped Y_2O_3 with 405 CW laser modulated at 50 ms pulse length; It is worth noting here the long lifetime of $^4F_{9/2}$ and $^4S_{3/2}$ state in Fig. S5(C) is due to the CR process (power density is 16 W/cm^2).

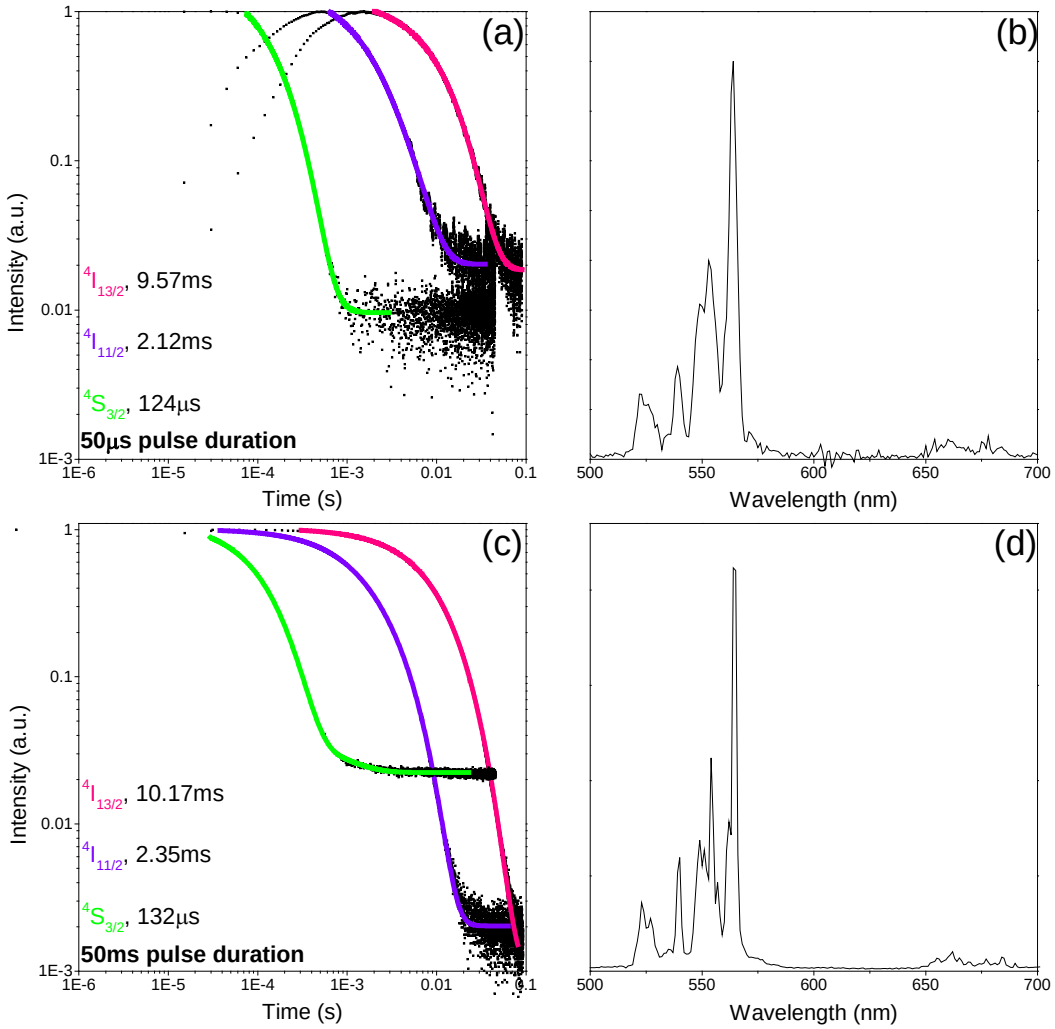

Fig. S6. (a) Intensity decay curves of $^4I_{13/2}$, $^4I_{11/2}$, $^4F_{9/2}$ and $^4S_{3/2}$ states of 0.2% Er^{3+}-doped Y_2O_3 with 405 CW laser modulated at 50us pulse length; (b) emission spectrum of 0.2% Er^{3+}-doped Y_2O_3 with 405 CW laser modulated at 50us pulse length; (c) intensity decay curves of $^4I_{13/2}$, $^4I_{11/2}$, $^4F_{9/2}$ and $^4S_{3/2}$ states of 0.2% Er^{3+}-doped Y_2O_3 with 405 CW laser modulated at 50 ms pulse length; (d) emission spectrum of 0.2% Er^{3+}-doped Y_2O_3 with 405 CW laser modulated at 50 ms pulse length (power density is 16 W/cm^2).

Emission Wavelength (nm)	0.2% Er^{3+}-doping		10% Er^{3+}-doping	
	50 µs	50 ms	50 µs	50 ms
1535	0.00957	0.01017	0.00144	0.00157
980	0.00212	0.00235	9.07×10^{-4}	0.00114
660			2.62×10^{-5}	4.48×10^{-4}
560	1.24×10^{-4}	1.32×10^{-4}	1.49×10^{-5}	1.80×10^{-4}

Table S2. Average decay times of the emitting states of the 0.2% and 10% Er^{3+}-doped Y_2O_3 samples under 405 nm excitation for the corresponding laser pulse durations. Numbers (in seconds) correspond to empty symbols in figure 3 (power density is 16W/cm^2).

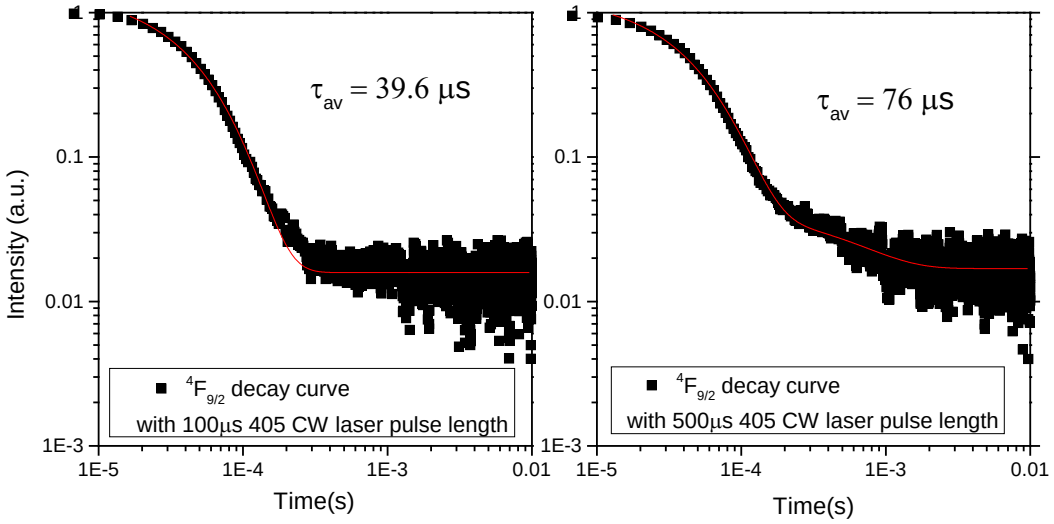

Figure S7. The lifetime of $^4F_{9/2}$ state under different laser pulse length (power density is 16 W/cm^2).

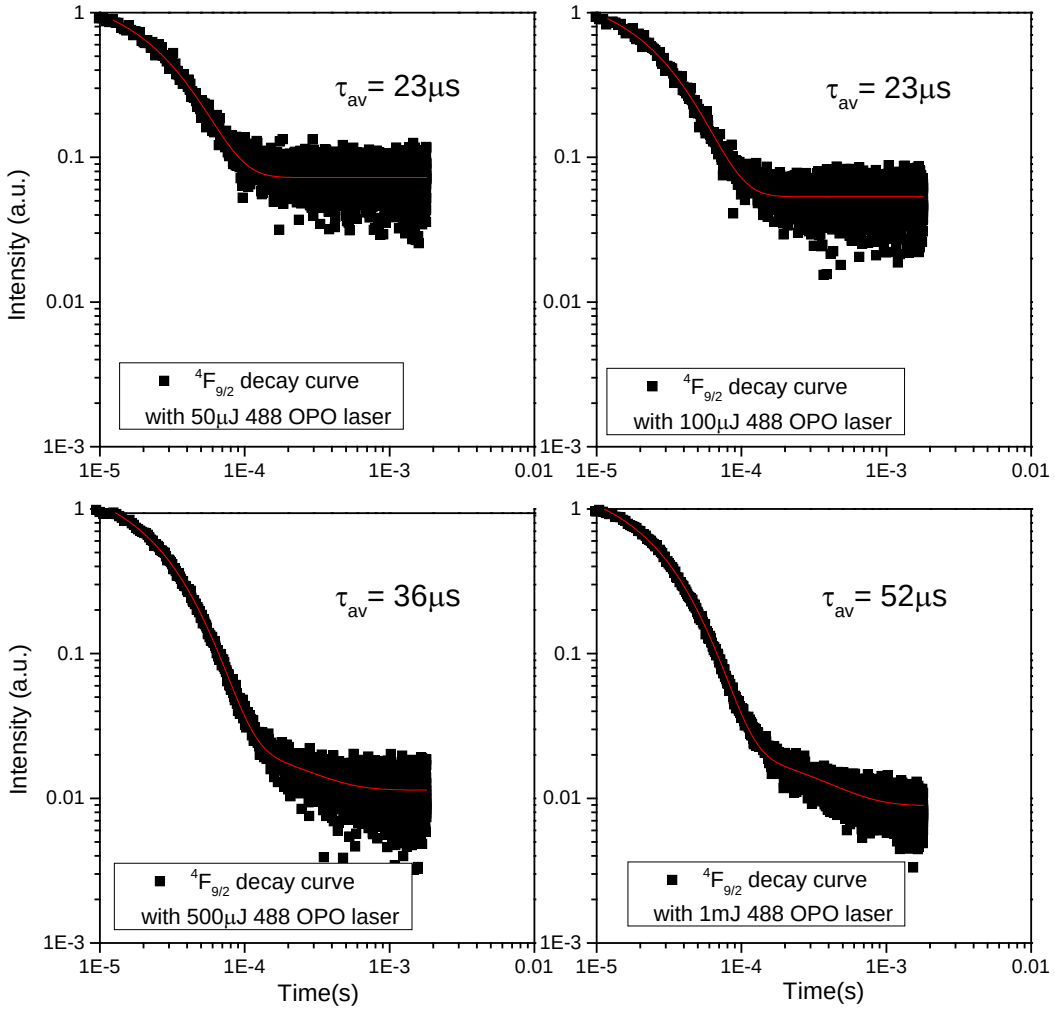

Figure S8. The lifetime of $^4F_{9/2}$ state under different laser power.

488 nm OPO laser excitation power (approx. power density)	Average decay time at 660 nm of 10% Er^{3+}-doped Y_2O_3
50 μJ ($1.5\times10^5 W/cm^2$)	2.32×10^{-5}
100 μJ ($3\times10^5 W/cm^2$)	2.30×10^{-5}
500 μJ ($1.5\times10^6 W/cm^2$)	3.56×10^{-5}
1 mJ ($3\times10^6 W/cm^2$)	5.16×10^{-5}
1.2 mJ ($3.6\times10^6 W/cm^2$)	6.50×10^{-5}

Table S3. Average decay time (in second) of the 10% Er-doped Y_2O_3 red emission under variable excitation powers (OPO excitation at 488 nm).

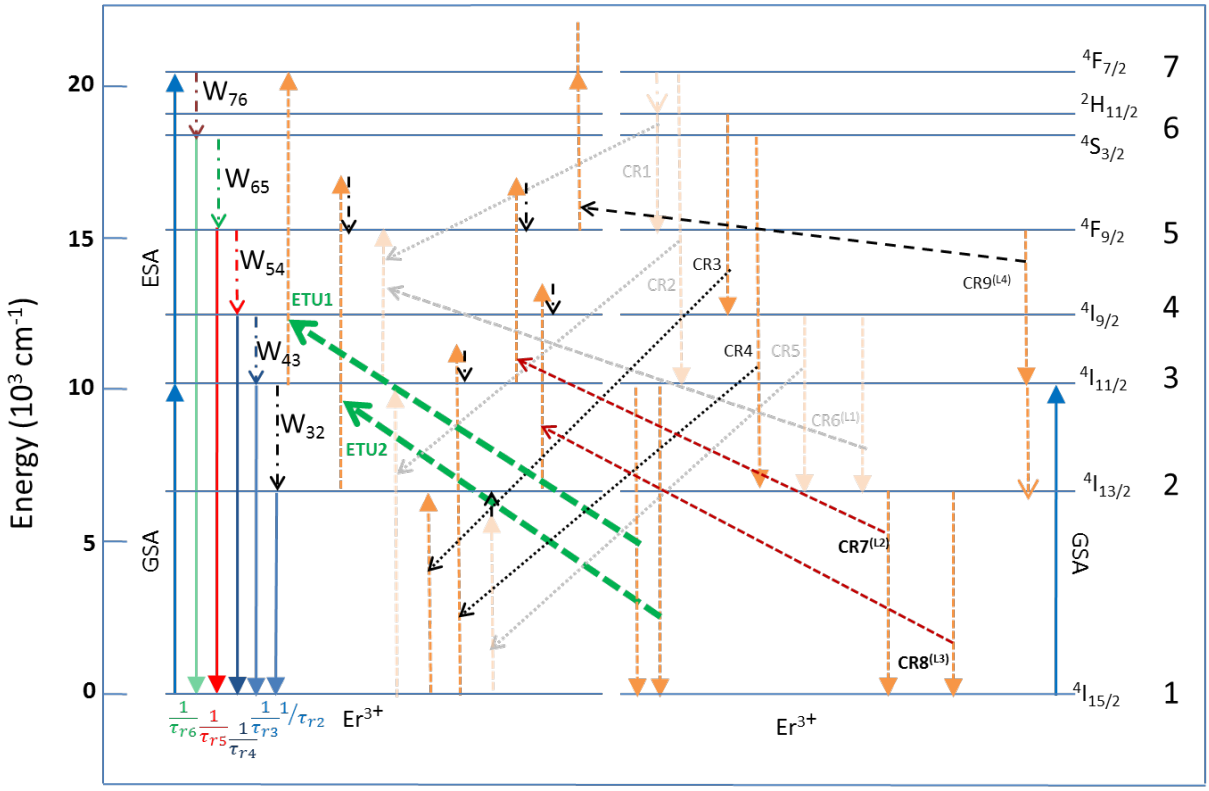

Figure S9. Significant energy transfer processes of the coupled Er^{3+} systems. See below and the main text for a description and interpretation of the τ_{ri} and W_{ij} parameters. Note that only the lower lying-states of the Er^{3+} configurations are considered, as our experiments can be considered low pumping power conditions (no significant spectral or dynamic changes are observed upon varying the UC powers, nor involving a higher population of the higher-lying states (with excitation at 378 nm)).

$\dot{n}_6 = -\frac{n_6}{\tau_{r6}} - W_{65}n_6 + W_{76}n_7 + W_{ETU1}n_3^2 + W'_{CR9}n_5^2 - W_{CR3}n_6n_1 - W_{CR4}n_6n_1$	(S1)
$\dot{n}_5 = -\frac{n_5}{\tau_{r5}} - W_{54}n_5 + W_{65}n_6 + W_{ETU2}n_3n_2 + W_{CR7}n_3n_2 - 2W_{CR9}n_5^2$	(S4)
$\dot{n}_4 = -\frac{n_4}{\tau_{r4}} - W_{43}n_4 + W_{54}n_5 + -W_{CR3}n_6n_1 + W_{CR8}n_2^2$	(S3)
$\dot{n}_3 = -\frac{n_3}{\tau_{r3}} - W_{32}n_4 + W_{43}n_4 + W_{CR4}n_6n_1 + W''_{CR9}n_5^2 - 2W_{ETU1}n_3^2 - W_{ETU2}n_3n_2 - W_{CR7}n_3n_2$	(S4)
$\dot{n}_2 = -\frac{n_2}{\tau_{r2}} + W_{32}n_3 + W_{CR9}n_5^2 + W_{CR3}n_6n_1 - W_{ETU2}n_3n_2 - 2W_{CR8}n_2^2 - W_{CR7}n_3n_2$	(S5)
$\dot{n}_1 = \frac{n_2}{\tau_{r2}} + \frac{n_3}{\tau_{r3}} + \frac{n_4}{\tau_{r4}} + \frac{n_5}{\tau_{r5}} - W_{ETU1}n_3^2 - W_{ETU2}n_3n_2 - W_{CR3}n_6n_1 - W_{CR4}n_6n_1 - W_{CR7}n_3n_2 - 2W_{CR8}n_2^2$	(S6)

Table S4. Dynamic differential equations corresponding to the population of the coupled Er^{3+} states with the active energy transfers and decays as labelled in figure S9 after illumination.

The radiative decay probability (per unit time) of a corresponding state *i* is given as $1/\tau_i$.

W_{ij} represents the radiative and non-radiative probability per unit time of a state decaying to the immediately lower-lying one. $1/\tau_i = 1/\tau_{ri} + \sum_j W_{ij}$. τ_{ri} and τ_i (or equivalently, W_{ij}) depend only on the host matrix and temperature, being irrespective of the Er^{3+} concentration (and thus are dominant for very diluted systems and can be derived from absorption and time-resolved spectroscopy). The approximations W_{ij} is negligible (<<) for $i > j+1$, $W_{ij} = W_{76}$ for $i > 6$, $W_{21} <<$ have been included above, (even in the cases of significant branching ratio parameters for a given couple of levels, etc.)

The probability per unit time of a CR process CRk is given by the corresponding rate W_{CRk} and, similarly, for ETU processes, W_{ETUk} is the corresponding rate.

Other departing approximations include $W_{CRk}<<$ for cross-relaxations labelled CRk, if involve the energy transfer from a level i and $1/\tau_i$ is considerably high. They will not affect significantly the dynamics, in comparison to other processes. This involves the faded processes depicted in figure S9.

Further approximations can be made considering the reduced value of W_{CR9}, quantifying the concentration quenching CR processes depopulating the red emitting state, which is often neglected in the literature and as it can be observed that, for the given excitation conditions, it is not very significant for the 0.5 to approx. 2% Er^{3+} concentration range in the Er^{3+}-doped Y_2O_3 system, so for

these concentrations, the grey terms can be neglected, but not necessarily all of them for higher concentrations.

Importantly, ETU2 and CR7$^{(L2)}$ processes are indistinguishable, as both involve equivalent Er^{3+} pairs so a further simplification can be made $W_{ETU2} + W_{CR7} = W_{II}$, irrespective of the erbium concentration.

As discussed in the main text, from the observed spectroscopic behaviour, we can determine that W_{CRi}, W_{ETUj} are considerably small for 0.2% Er^{3+}-doped Y_2O_3, although at least W_{ETU1} and W_{II} ($W_{II} = W_{ETU2} + W_{CR7(L2)}$) become important for Er^{3+} concentrations higher than 0.5% in the Er^{3+}-doped Y_2O_3 system for the studied excitation conditions. This implies these mechanism are the driving processes for the UC for Er^{3+} concentrations higher than 6.71×10^{19} Er^{3+} ions / cm^3, in this matrix.

Also, over the studied Er^{3+}concentrations range and excitation conditions, τ_4 is considerably small and $W_{43}n_4$ can be considered dominant. The term in $W_{65}n_6$ can also be considered small, as in the DC / ESA processes, the red emission is very much negligible in comparison with the green one. This approximation is considered in the main text when discussion the photoluminescence properties for Er^{3+} concentrations 0.5% and higher. It implies that $W_{ETU2} + W_{CR7} = W_{II}$ is the dominant term for populating the $^4F_{9/2}$ state (level 5, red emission) in UC and, together with other looping mechanisms, contribute to the distinct behaviour of the emission of this state (see main text).

The solution of the equations under the consideration that CR3, CR4 are not significant, and that energy transfer from $^4I_{11/2}$ (state 3) is much smaller than the decay constant, $1/\tau_3 >> 2W_{ETU1}n_3^2 + W_{II}n_3n_2$+…, leads [see Ref. 21, from the main text] to an asymptotic temporal decay of $^4F_{9/2}$ (level 5, red emission) $1/\tau_{av5} = 1/\tau_2 + 1/\tau_3 \approx 1/\tau_3$, and a corresponding $\tau_{av6} = \tau_3/2$ for $^4S_{3/2}$ (level 6, green emission) . This is exactly what we observe in the 0.5-2% concentration range (see Figure 3 in the text, table S1 above), also note that the DC lifetimes are similar for the excitation conditions.

Importantly, as described in the text, the above approximation is no longer valid for Er^{3+} concentrations higher than 5%, in the excitation conditions so CR mechanisms become severe, and the average decay constant decreases. This causes also differences in the DC lifetimes, which (for given excitation conditions) are observed to increase in the case of the $^4F_{9/2}$ (level 5, red emission). This is assigned, as described in the text, to the influence of looping mechanisms feeding the red-emitting state from longer-lived lower-lying reservoirs. These mechanism also affect the DC lifetime in other excitation conditions (see main text and above, e.g. tables S2 and S3).

The above analysis of the CR and ET mechanisms that describe the dynamic and spectral behaviour in the DC and UC processes have important consequences not only in the general case concentrated Er^{3+} systems but, importantly, in the case of Er^{3+}/Yb^{3+} co-doped systems, not only because in most of practical systems the Er concentration is typically higher than 6.71×10^{19} Er^{3+} ions / cm^3 (for $NaYF_4$: 2% Er, 20% Yb, for instance, it is more than 10^4 times that, in the order of 10^{24} Er^{3+} ions / cm^3), but also because the analogous ET mechanisms from the much more absorbing Yb^{3+} ions, whose excited energy is similar to our excitation energies, will be considerable.